

# Current-induced re-entrant superconductivity and extreme nonreciprocal superconducting diode effect in valley-polarized systems

Yu-Chen Zhuang<sup>1</sup> and Qing-Feng Sun<sup>1,2,\*</sup>

<sup>1</sup>*International Center for Quantum Materials, School of Physics, Peking University, Beijing 100871, China*

<sup>2</sup>*Hefei National Laboratory, Hefei 230088, China*

(Dated: January 3, 2025)

The superconducting diode effect (SDE) refers to the nonreciprocity of superconducting critical currents for the metal-superconductor transition. Generally, the SDE has a positive and a negative critical currents  $j_{c\pm}$  corresponding to two opposite directions whose amplitudes are unequal. It is demonstrated that an extreme nonreciprocity where two critical currents can become both positive (or negative) has been observed in a recent experiment. In this work, we theoretically propose a possible mechanism to realize an extreme nonreciprocal SDE. Based on a microscopic theory and a simple valley-polarized model, we demonstrate that depairing currents required to dissolve Cooper pairs can be remodulated under the interplay between the valley polarization and the applied current. Near the disappearance of the superconductivity, the remodulation is shown to induce the extreme nonreciprocity and also the current-induced re-entrant superconductivity where the system has two different critical current intervals. Our study may provide new horizons for understanding the coexistence of superconductivity and spontaneous ferromagnetism and pave a new way to designing the SDE with 100% efficiency.

## I. INTRODUCTION

Superconducting diode effect (SDE) is a recently observed superconducting phenomenon with a nonreciprocity of the non-dissipative supercurrent [1, 2], and has been attracting substantial attention. Such nonreciprocity means amplitudes of critical currents required to destroy the superconductivity are unequal in opposite directions. As a new transport phenomenon, SDE not only can uncover underlying features in exotic superconducting systems, but also serves as a non-dissipative circuit, which has promising applications in superconducting electronics [3], superconducting spintronics [4], quantum information and communication technology [5, 6]. Since the observation of SDE in artificial superlattice  $[\text{Nb}/\text{V}/\text{Ta}]_n$  [7], similar nonreciprocity of supercurrents has been observed in series of experiments, including bulk materials of diverse dimensions [8–13], Josephson junction devices [14–21], engineered superconducting structures [22, 23]. In theory, the rise of SDE generally relies on simultaneous breaking of time-reversal symmetry (TRS) and inversion symmetry, which is closely related to magnetochiral anisotropy [24–28], and finite-momentum Cooper pairing [29–32].

The performance of the SDE can be measured by the superconducting diode efficiency  $\eta = \frac{j_{c+} - |j_{c-}|}{j_{c+} + |j_{c-}|}$ , with the critical currents  $j_{c\pm}$  for positive and negative directions [1]. The value of  $\eta$  generally depends on the relevant system parameters like working temperature, applied magnetic field and chemical potentials [28, 33–35]. In most experiments,  $\eta$  is optimized to several tens of percent. One notable exception appears in a recent experiment for zero-field SDE in small-twist-angle trilayer graphene

where critical currents  $j_{c\pm}$  are found to cross zero and become both positive or negative near the end of superconducting regime [12]. This so-called extreme nonreciprocity indicates a realization of SDE with 100% efficiency [36]. It is a very counterintuitive feature since the electric current does not destroy superconductivity as traditionally believed, but rather promotes a normal state into a superconducting state. Some recent theoretical studies implies that the significant enhancement of  $\eta$  possibly come from the coupling between the symmetry-breaking order parameter and supercurrents [37], or dissipations induced by the out-of plane electric field [36].

In twisted graphene systems, a non-negligible phenomenon is that a dc current can modulate and even switch the valley polarization [38–43]. From the view of the bulk transport, the applied current can redistribute electron occupations in different valley bands near the Fermi level, and then induce energy band shifts due to the Coulomb interaction [40]. Considering the spontaneous valley polarization plays an important role in the SDE in twisted trilayer graphene, it is worth investigating the connection between the extreme nonreciprocal SDE and the current-induced valley polarization modulation.

In this work, based on the current-induced valley polarization modulation, we theoretically propose a possible mechanism to achieve the extreme nonreciprocity. By a simple valley-polarized system with intervalley pairings, we first study the nonreciprocity of intrinsic depairing current  $\tilde{j}_c$  which is demanded to dissolve flowing Cooper pairs [33]. Because of the interplay between the current and valley occupations, we point out  $\tilde{j}_c$  should be further remodulated to the actual critical current  $j_c$ . In a large valley splitting regime close to the disappearance of superconductivity, this remodulation could lead to extreme nonreciprocity. The effects of variations of fillings and external magnetic fields on  $j_c$  are also investigated. Moreover, we raise a new phenomenon, the

\* sunqf@pku.edu.cn

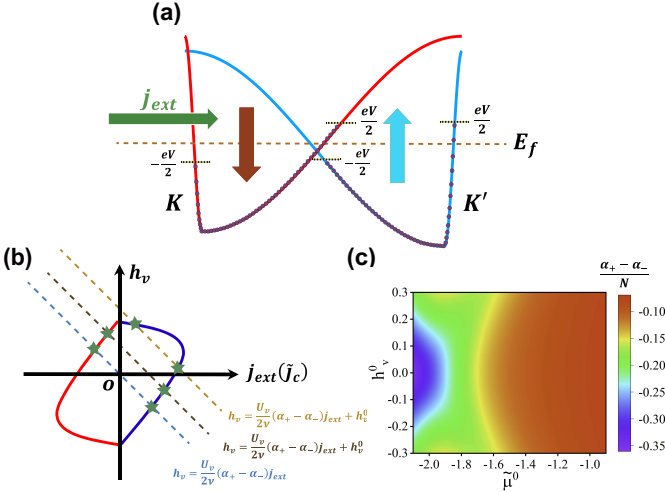


FIG. 1. (a) Schematic illustration for the mechanism of the current-induced valley polarization modulation. The red line and cyan line denote the  $K'$  valley and  $K$  valley, respectively. The purple dots denote the electron occupations on energy bands. The red and cyan arrows indicate the variation of valley splitting induced by an applied current  $j_{ext}$ . (b) Depairing currents  $\tilde{j}_{c\pm}$  (dark blue and red solid lines) versus valley splitting field  $h_v$ . The colored dashed lines denote different  $h_v - j_{ext}$  curves. (c) The colormap for the coefficient  $(\alpha_+ - \alpha_-)/N$  versus the initial valley splitting field  $h_v^0$  and initial modified chemical potential  $\tilde{\mu}^0$ .

current-induced re-entrant superconductivity, where the system has two different superconducting regions with distinct critical current intervals. Our study provides a possible routine to achieve SDE with 100% efficiency and also sheds light on the extreme nonreciprocity observed in the recent experiment.

The remainder of this article is organized as follows. In Sec. II, we construct a microscopic model to describe the spontaneous valley polarizations. In Sec. III, based on the model in Sec. II, we further give a physical mechanism to illustrate the current-induced valley polarization modulation. In Sec. IV, we study superconducting depairing currents and present a physical picture to demonstrate how intrinsic depairing currents are remodulated to actual critical currents. In Sec. V, with a specific model, we use numerical calculations to verify the proposed physical picture. The variations of actual critical currents with electron parameters and external magnetic fields are also studied in detail. In Sec. VI, we give some discussions and a conclusion. The detailed formulations of the current-induced valley polarization modulation are shown in Appendix A. In Appendix B, we give some theoretical discussions to evaluate the self-consistent manner due to the effect of applied currents. Some additional studies about the effect of band asymmetry and the system size are put in Appendix C and D.

## II. THE INTERACTION-INDUCED VALLEY POLARIZATION

We consider a two-band Hamiltonian to implement a valley-polarized system with an intervalley interaction:

$$H^v = \sum_{k,\tau} (\epsilon_{k,\tau} - \mu) c_{k,\tau}^\dagger c_{k,\tau} + \frac{U_v}{\mathcal{V}} \sum_{k,k'} c_{k,+}^\dagger c_{k,+} c_{k',-}^\dagger c_{k',-}, \quad (1)$$

where  $\tau = \pm$  label the valley index  $K, K'$ ,  $U_v > 0$  denotes the repulsive intervalley interaction.  $\mathcal{V}$  and  $\mu$  are the systemic size and chemical potential.  $\epsilon_{k,\tau}$  denotes the single-particle band, which satisfies TRS:  $\epsilon_{k,+} = \epsilon_{-k,-}$ . Taking the mean-field approximation, the Hamiltonian becomes  $H_{MF}^v = \sum_{k,\tau} E_{k,\tau} c_{k,\tau}^\dagger c_{k,\tau} + \text{const}$  where  $E_{k,\tau} = \epsilon_{k,\tau} - \mu + \frac{U_v}{\mathcal{V}} n_{-\tau}$  with  $n_\tau = \sum_k \langle c_{k,\tau}^\dagger c_{k,\tau} \rangle = \sum_k f(E_{k,\tau}) = 1/(1 + e^{\frac{E_{k,\tau}}{T}})$  is the Fermi distribution. The const =  $-\frac{U_v}{\mathcal{V}} n_+ n_-$  is a constant arising from the mean-field approximation. This model is similar to the rigid band flavor Stoner model with a  $SU(4)$  symmetric Coulomb interaction energy  $V_{int} \propto \sum_{\alpha \neq \beta} n_\alpha n_\beta$  ( $\alpha, \beta$  denote four flavors  $K \uparrow, K \downarrow, K' \uparrow, K' \downarrow$ ), which is used to study flavor polarizations in graphene [44–46]. In light of implications in the experiment [12], we here first focus on valley flavors and neglect spin flavors.

It is easy to find that the growth of the electron occupation  $n_\tau$  could lift the energy of  $-\tau$  valley, and thus influence the total free energy  $F_v$  of the system:

$$F_v(n, m) = -T \sum_{k,\tau} \ln(1 + e^{-\frac{E_{k,\tau}}{T}}) - \frac{U_v}{4\mathcal{V}} (n^2 - m^2) + \mu n, \quad (2)$$

where  $n = n_+ + n_-$  is the total electron occupation,  $m = n_+ - n_-$  denotes the valley polarization and  $T$  is the temperature of the system. Generally, the system is fixed with a definite total electron occupation  $n$  and reaches a state where  $m$  is just the minimum point of the free energy  $F_v(n, m)$ . Therefore, the valley polarization can be solved by:

$$\frac{\partial F_v}{\partial m} = \frac{U_v}{2\mathcal{V}} \left( m - \sum_{k,\tau} \frac{\tau}{1 + e^{\frac{E_{k,\tau}}{T}}} \right) = 0. \quad (3)$$

Once  $U_v g(E_f)/\mathcal{V} > 1$  where  $g(E_f)$  is the density of states at the Fermi level  $E_f$ , the strong repulsive Coulomb interaction overwhelms the kinetic energy and make the system favor a nonequal electron distribution between two valleys. This is analogous to the well-known Stoner criterion and at this time the solution  $m$  in Eq. (3) is nonzero [47]. The spontaneous valley polarization further introduces a valley splitting field  $h_v = \frac{U_v m}{2\mathcal{V}}$  and a modified chemical potential  $\tilde{\mu} = \mu - \frac{U_v n}{2\mathcal{V}}$  in mean-field bands  $E_{k,\tau} = \epsilon_{k,\tau} - \tilde{\mu} - h_v \tau$ . [see a schematic illustration for red and cyan solid lines in Fig. 1(a)].

### III. THE CURRENT-INDUCED VALLEY POLARIZATION MODULATIONS

In twisted graphene systems, it is found that a dc current could modulate and even switch the valley polarization [38–43]. We here illustrate it from a nonequilibrium ballistic quantum transport. In Fig. 1(a), under an external bias  $V$ , an applied current  $j_{ext}$  flows from the source to drain. The Fermi level of electrons with positive (negative) velocities will rise (fall)  $\frac{eV}{2}$ , compared to the Fermi level  $E_f$  in equilibrium [48]. Considering intravalley inversion symmetry-broken bands ( $\epsilon_{k,\tau} \neq \epsilon_{-k,\tau}$ ), the variation of electron occupation for opposite velocities cannot be offset due to unequal density of states at the Fermi level (indicated by purple dots on colored solid lines). Thus,  $n_\tau$  will change in each valley and is proportional to  $j_{ext}$  at a small bias  $V$  (see detailed derivations in Appendix A):

$$n_\tau = n_\tau^0 + \alpha_\tau j_{ext}. \quad (4)$$

The coefficient  $\alpha_\tau$  is a function of the modified chemical potential  $\tilde{\mu}$  and also the valley splitting field  $h_v$ . It relies on the difference between the positive and negative Fermi velocities and will be zero once  $\epsilon_{k,\tau} = \epsilon_{-k,\tau}$  (see Appendix A). This is well consistent with our picture shown in Fig. 1(a).

The variation of  $n_\tau$  will further alter valley polarization  $m = n_+ - n_-$  and the valley splitting field:

$$h_v = \frac{U_v}{2\mathcal{V}} m = \frac{U_v}{2\mathcal{V}} (\alpha_+ - \alpha_-) j_{ext} + h_v^0. \quad (5)$$

Here  $h_v^0$  are the initial valley splitting field at  $j_{ext} = 0$ . It should be noted that the linear relation in Eq. (5) is only an approximation. In principle, the applied current  $j_{ext}$  which redistributes electron occupations on each valley can also refresh the value of  $h_v^0$  simultaneously. The rigorous self-consistent calculation of  $h_v^0$  including the nonequilibrium electric current is a subtle question. For simplicity, we focus on a small current range where the impact of  $j_{ext}$  on  $h_v^0$  should be minor (see further discussions in Appendix B). And thus in the calculations, we just ignore the influence on  $h_v^0$  on the right side of Eq. (5) by the effect of  $j_{ext}$ .

The breaking of intravalley inversion symmetry on the energy bands could naturally exist in twisted graphene systems [40], as well as some materials with trigonal warping on the Fermi surface [49]. Additionally, TRS guarantees opposite signs of  $\alpha_\pm$ . See Fig. 1(a),  $j_{ext}$  could make  $n_-$  larger and  $n_+$  smaller, reducing the valley polarization  $m$  and valley splitting field  $h_v$  (denoted by red and cyan arrows).

### IV. THE PHYSICAL PICTURE FOR THE EXTREME NONRECIPROCITY

By the valley-polarized system shown in Sec. II, now we add an s-wave intervalley pairing originating from an

effective attraction. Although the coexistence between valley ferromagnetism and superconductivity is rare, similar traits have been found in twisted graphene systems [12, 50]. We consider a Bogoliubov-de Gennes (BdG) Hamiltonian [33, 34]:

$$H(q) = \sum_{k,\tau} E_{k,\tau} c_{k,\tau}^\dagger c_{k,\tau} + \sum_k \Delta(q) c_{k+q,+}^\dagger c_{-k+q,-}^\dagger + \text{H.c.} \quad (6)$$

Here  $2q$  denotes the center-of-mass momentum of the Cooper pair reflecting a helical state or Flude-Fellel state  $\Delta(x) = \Delta e^{i2qx}$  [33, 34, 51]. Note that there is also a constant:  $\text{const} = \sum_k E_{-k+q,-} + \frac{\mathcal{V}}{U_s} \Delta^2(q)$  in Eq. (6) arising from the mean-field approximation. It does not affect the self-consistent calculation but will affect the superconducting free energy. Using BdG transformation, the Hamiltonian  $H(q)$  can be diagonalized as  $H(q) = \sum_k \tilde{E}_+(k, q) \alpha_{k+q}^\dagger \alpha_{k+q} + \tilde{E}_-(k, q) \beta_{-k+q} \beta_{-k+q}^\dagger$  where  $\tilde{E}_\pm(k, q) = E_1(k, q) \pm \sqrt{E_2^2(k, q) + \Delta^2(q)}$  is the eigenvalues with  $E_{1,2}(k, q) = (E_{k+q,+} \mp E_{-k+q,-})/2$ . For every fixed  $q$ ,  $\Delta(q)$  can be self-consistently determined by a gap equation [33]:

$$\begin{aligned} \Delta(q) &= -\frac{U_s}{\mathcal{V}} \sum_k \langle c_{-k+q,-} c_{k+q,+} \rangle \\ &= -\frac{U_s}{\mathcal{V}} \sum_k \frac{\Delta(q)}{2\sqrt{E_2^2(k, q) + \Delta^2(q)}} (\langle \alpha_{k+q}^\dagger \alpha_{k+q} \rangle - \langle \beta_{-k+q} \beta_{-k+q}^\dagger \rangle) \\ &= -\frac{U_s}{\mathcal{V}} \sum_k \frac{\Delta(q)}{2\sqrt{E_2^2(k, q) + \Delta^2(q)}} [f(\tilde{E}_+(k, q)) - f(\tilde{E}_-(k, q))]. \end{aligned} \quad (7)$$

Here  $U_s$  represents the magnitude of effective electron-electron attraction. Based on  $\Delta(q)$  in Eq. (7), we can evaluate the free energy  $\Omega(q)$  per volume:

$$\Omega(q) = \frac{\Delta^2(q)}{U_s} + \frac{1}{\mathcal{V}} \sum_k E_{-k+q,-} - \frac{T}{\mathcal{V}} \sum_{\pm} \ln(1 + e^{\frac{-\tilde{E}_\pm(k, q)}{T}}). \quad (8)$$

Following the previous derivations [33], the superconducting current flowing through the system  $j_s$  satisfies:

$$\begin{aligned} j_s(\Delta(q), q) &= \frac{e}{\hbar} \partial_q \Omega(\Delta(q), q) \\ &= \frac{e}{\hbar} \partial_q [\Omega(\Delta(q), q) - \Omega(\Delta(q) = 0, q = 0)] \quad (9) \\ &= \frac{e}{\hbar} \partial_q F_s(q). \end{aligned}$$

$F_s(q) = \Omega(\Delta(q), q) - \Omega(\Delta(q) = 0, q)$  is the condensation energy per volume to quantize the difference of free energy density between the superconducting state and the normal state. In addition, the last equation uses the fact that  $\Omega(\Delta(q) = 0, q) = \Omega(\Delta(q) = 0, q = 0)$ . Note that once  $F_s(q) > 0$ , we set it as zero considering the superconducting phase is no longer stable. Eq. (9) actually follows the standard expression  $j_s = -\partial_A \Omega$  with the gauge vector  $A$ , since  $q$  changes by  $-\delta A$  when  $A$  changes  $\frac{e}{\hbar} \delta A$  [33, 34]. In addition, the depairing currents  $\tilde{j}_{c\pm}$  just

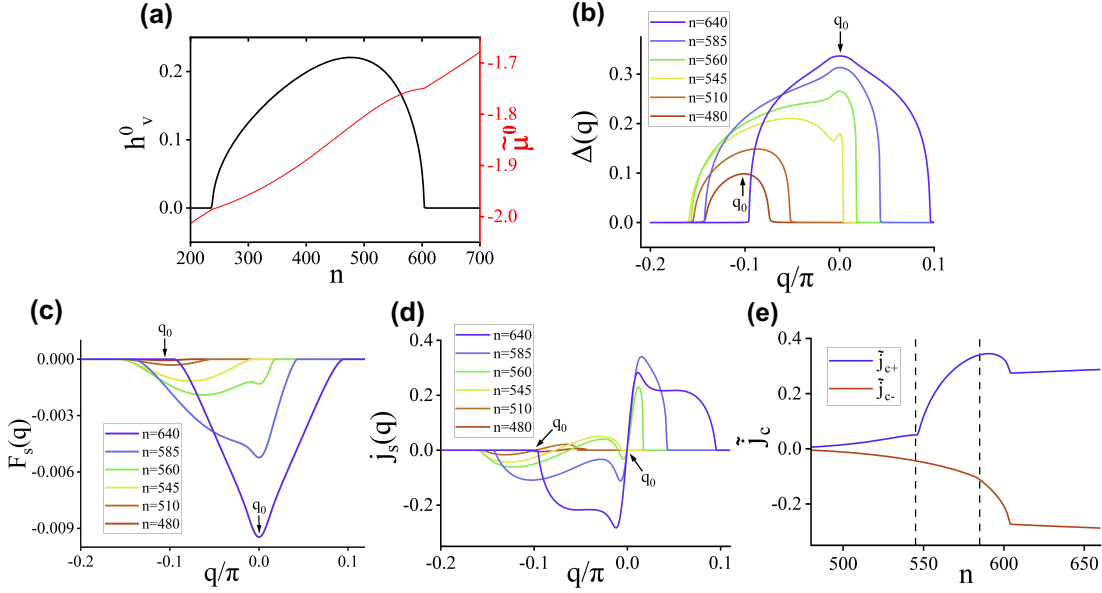


FIG. 2. (a) The initial valley splitting field  $h_v^0$  (dark line) and initial modified chemical potential  $\tilde{\mu}^0$  (red line) versus the electron occupation  $n$ . (b, c, d) The distribution of superconducting order parameter  $\Delta(q)$ , the condensation energy  $F_s(q)$  and supercurrent  $j_s(q)$  for several  $n$ . (e) The variation of intrinsic depairing currents  $\tilde{j}_{c\pm}$  with the filling  $n$ .

corresponds the global maximum  $\tilde{j}_{c+} = \max_q[j_s(q)]$  and the global minimum  $\tilde{j}_{c-} = \min_q[j_s(q)]$ , respectively.

For the usual case, the depairing currents are just equal to critical currents which break the superconductivity. No superconducting state can sustain once the applied current  $j_{ext} > \tilde{j}_{c+}$  or  $j_{ext} < \tilde{j}_{c-}$  for a definite valley polarization  $h_v$  [33]. However, the situation becomes more complex including the effect of the current-induced valley polarization modulation. See colored dashed lines Fig. 1(b), as the applied current  $j_{ext}$  varies, the  $h_v$  will also change following the relation shown in Eq. (5). Note that  $h_v$  affects the depairing currents  $\tilde{j}_{c\pm}(h_v)$  simultaneously (colored solid lines). Therefore, the values of  $j_{ext}$  and  $\tilde{j}_{c\pm}$  should be recompared. In Fig. 1(b), we use dark green stars to denote intersection points between the  $h_v - j_{ext}$  line (dashed lines) and the  $\tilde{j}_{c\pm} - h_v$  lines (solid lines). At the regions between these intersections,  $|j_{ext}|$  is always smaller than  $|\tilde{j}_{c\pm}|$ , which means the system can stay in superconducting phase. While in the other regions for  $j_{ext} > \tilde{j}_{c+}$  or  $j_{ext} < \tilde{j}_{c-}$ , the superconducting phase cannot exist. Therefore, the intersection points actually denote the actual critical currents  $j_{c\pm}$  in metal-superconductor transitions. Moreover, we can find the characteristics of  $j_{c\pm}$  strongly depends on the initial valley splitting field  $h_v^0$ . One notable example is that the system stays in the normal phase at  $j_{ext} = 0$ , but is driven into a superconductor when  $j_{ext} > 0$ . This is characterized by both  $j_{c\pm} > 0$  (dark green stars on the earthy yellow line), which exactly corresponds extreme nonreciprocity observed in previous experiment [12].

When the dependence between  $j_{ext}$  and  $h_v$  disappears ( $\alpha_+ - \alpha_- = 0$ ), the situation just goes back to the trivial case where  $j_{c\pm} = \tilde{j}_{c\pm}$ . So, the key point of our theory

is the current-induced valley polarization modulation in Eq. (5). It is noted that our theory is not aimed to give a comprehensive description of the behavior for currents. Actually, when the system has become a superconducting state, the physical picture shown in Fig. 1(a) and Eq. (5) will be invalid due to a screening of the electric voltage. Therefore, the behavior for currents within superconducting phases may not be well described by our theory. But we emphasize that predictions on actual critical currents  $j_c$  are still valid, since the predicted normal phases outside the intersection points still make sense in Fig. 1(b). The actual critical currents  $j_{c\pm}$  are just the end of these valid regions (dark green stars), which well denote the phase boundaries from normal phases to superconducting phases.

A larger coefficient  $\alpha_+ - \alpha_-$  implies  $I_{ext}$  can weaken  $h_v$  more quickly and may drive the system into superconducting phase more easily. Below we choose one simple 1D model with  $\epsilon_{k,+} = -2t \cos[\frac{8}{15}(k - \frac{7\pi}{8})]$  for  $-\pi \leq k \leq \frac{7\pi}{8}$ ,  $\epsilon_{k,+} = -2t \cos(8k - \pi)$  for  $\frac{7\pi}{8} < k < \pi$ , and  $\epsilon_{k,+} = \epsilon_{-k,-}$ . This model can capture the asymmetric features of low-energy bands in twisted graphene [40]. In numerical calculations,  $\mathcal{V} = Na$  with a periodic boundary condition and  $N = 2000$ .  $t = 1$ ,  $\frac{e}{\hbar}t = 1$ , and  $a = 1$  are set as energy, current and length units, respectively. We also set  $U_v = 2.8$ ,  $U_s = 1.86$  and temperature  $T = 0.1$ . In Fig. 1(c), the coefficient  $(\alpha_+ - \alpha_-)/N$  versus the initial  $h_v^0$  and  $\tilde{\mu}^0$  is shown [52].  $(\alpha_+ - \alpha_-)/N$  dives as  $\tilde{\mu}^0$  becomes lower, since Fermi velocities approach zero and  $\alpha_\tau$  becomes divergent near the band bottom. Additionally, the more asymmetrical the bands are, the larger  $\alpha_+ - \alpha_-$  is (see Appendix C), and in principle the easier the extreme nonreciprocity is realized.

## V. THE NUMERICAL CALCULATED RESULTS

In this section, we will use a series of numerical calculations to validate our physical pictures illustrated in Fig. 1. We first study the initial valley splitting field  $h_v^0$  and corresponding depairing currents  $\tilde{j}_{c\pm}$  without the effect of current-induced valley polarization modulation. Then, through the remodulation process in Fig. 1(b), we obtain actual critical currents  $j_c$  and explore the situation where the extreme nonreciprocity appears. We will also investigate the influence on  $j_c$  by the electron occupation  $n$  and the external magnetic field  $B$ .

### A. The calculations without the effect of current-induced valley polarizations

For a given electron occupation  $n$  (or filling factor  $\nu = n/N$ ), the initial  $\tilde{\mu}^0$  and  $h_v^0$  can be solved self-consistently from  $H_{MF}^v$  and are shown in Fig. 2(a). Notice that  $\pm h_v^0$  are degenerate solutions but we choose the positive one like the magnetic training in the experiment [12]. Here  $\tilde{\mu}^0$  naturally declines as  $n$  decreases. A non-zero  $h_v^0$  appears around  $240 < n < 600$ . Based on  $h_v^0$ , the  $\Delta(q)$  is solved from the self-consistent gap equation in Eq. (7), as shown in Fig. 2(b). As  $n$  declines from  $n = 640$  to  $n = 480$ ,  $h_v^0$  becomes stronger and  $\Delta(q)$  becomes weaker and more asymmetric with  $\Delta(q) \neq \Delta(-q)$ . This is because  $h_v^0$  breaks TRS and destroys the Cooper pairs from intervalley pairings. Especially, as  $n < 545$ , the strong  $h_v^0$  causes that the center of  $\Delta(q)$  wholly shifts from  $q_0 = 0$  to  $q_0 \approx -0.1\pi$ , which apparently suggests Cooper pairs have large non-zero center of mass momenta [Fig. 2(b)].

Based on  $\Delta(q)$ , we calculate corresponding condensation energy density  $F_s(q)$ , as shown in Fig. 2(c). As  $n$  changes from  $n = 640$  to  $n = 480$ , the initial valley splitting field increases to break TRS and intervalley pairing, thus  $F_s(q)$  becomes much more asymmetric and narrower. At around  $n = 480$ ,  $F_s(q)$  reaches almost zero and indicates superconductivity is highly unstable. Specially, a single-well structure of  $F_s(q)$  with one global minimum assigning the ground state at  $q_0 = 0$  ( $n = 640$ ) gradually evolves into a double-well structure under a moderate valley splitting field (e.g.  $n = 560$ ) with two local minimums. It goes back to the single-well structure with one minimum at  $q_0 \approx -0.1\pi$  under a high valley splitting field (e.g.  $n = 545$ ). Overall, the superconductor transforms from a ‘weak’ helical phase to a ‘strong’ helical phase as the valley splitting field climbs [35].

We also calculate supercurrents  $j_s(q)$  and depairing currents  $\tilde{j}_{c\pm}$  versus  $n$  [Figs. 2(d, e)]. For about  $n > 600$ ,  $j_s$  appears as an odd function with  $\tilde{j}_{c+} = -\tilde{j}_{c-}$  since the initial valley splitting field  $h_v^0$  is zero [Fig. 2(a)]. As  $n$  decreases,  $h_v^0$  climbs and  $j_s(q)$  becomes asymmetrical.  $|\tilde{j}_{c-}|$  gradually decays while  $\tilde{j}_{c+}$  lifts slightly because a small  $h_v^0$  gives Cooper pairs finite momenta to flow towards one

direction more easily [Fig. 2(e)]. By further decreasing  $n$ , two additional local extremums appear in  $j_s(q)$  around a relatively high momentum  $q_0 \approx -0.1\pi$  [Fig. 2(d)], and they successively become the new global minimum  $\tilde{j}_{c-}$  ( $n < 585$ ) and maximum  $\tilde{j}_{c+}$  ( $n < 545$ ) [denoted by black dashed lines in Fig. 2(e)]. Especially, the difference between  $\tilde{j}_{c\pm}$  appears to be tiny after a transition from the ‘weak’ helical phase in low  $h_v^0$  to the ‘strong’ helical phase in high  $h_v^0$ , see Figs. 2(c,d). This process are similar to results in Rashba-Zeeman superconductors [33, 35].

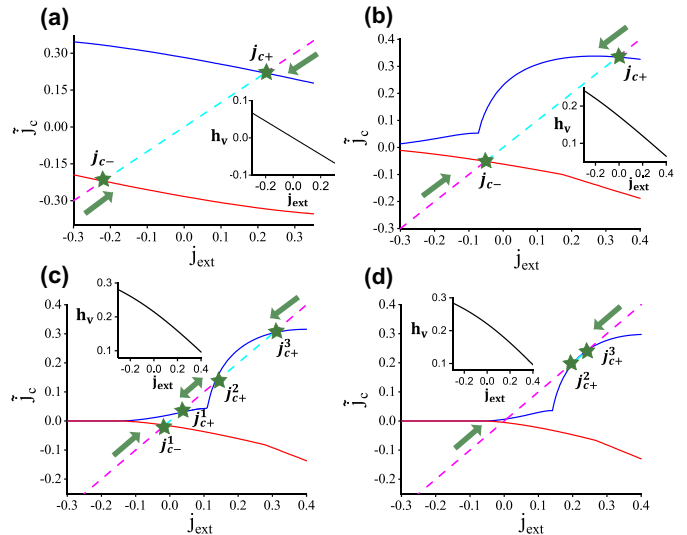


FIG. 3. (a-d) The depairing currents  $\tilde{j}_c$  (main panels) and  $h_v$  versus  $j_{ext}$  (insets) for  $n = 640$  (a),  $n = 560$  (b),  $n = 510$  (c) and  $n = 480$  (d). The intersection points (dark green stars) between the  $\tilde{j}_{c,\pm} - j_{ext}$  solid lines and  $\tilde{j}_c = j_{ext}$  dashed lines are  $j_c$ . On dashed lines, the magenta parts denote the regions of the normal phases where the physical picture in Fig. 1(a) is valid. The cyan parts denote the regions where the system eventually transitions into the superconducting phases and Fig. 1(a) is invalid. The dark green arrows denote the meta-superconductor transition where a normal state is driven by the applied current into a superconducting state.

### B. The actual critical currents through the remodulation process

Including the effect of current-induced valley polarization modulation, we state that depairing currents  $\tilde{j}_c$  can be further remodulated as the actual critical currents  $j_c$ . As illustrated in Fig. 1(b),  $j_c$  can be determined by intersection points between the curve  $\tilde{j}_c(h_v)$  and the curve  $h_v(j_{ext})$ . Note that  $j_{ext}$  and  $h_v$  have a definite relation in Eq. (5). Equivalently, we show diagrams with curves  $\tilde{j}_{c,\pm} - j_{ext}$  (colored solid lines) and curves  $\tilde{j}_c = j_{ext}$  (colored dashed lines) for four different  $n$  in Fig. 3.

In Fig. 3(a) with  $n = 640$ ,  $h_v^0$  is zero and depairing currents satisfy  $\tilde{j}_{c+} = -\tilde{j}_{c-}$  at  $j_{ext} = 0$ . A non-zero applied current  $j_{ext}$  can evolve  $h_v$  to finite [inset in Fig. 3(a)], and simultaneously affect  $\tilde{j}_{c\pm}$ . While, intersection points

still satisfy  $\tilde{j}_{c+} = -\tilde{j}_{c-}$  indicating no SDE (dark green stars), due to the fact that  $\tilde{j}_{c+}(h_v) = -\tilde{j}_{c-}(-h_v)$  and  $h_v(j_{ext}) = -h_v(-j_{ext})$ . When  $n = 560$ , a small  $h_v^0$  appears and  $\tilde{j}_{c+} \neq |\tilde{j}_{c-}|$  at  $j_{ext} = 0$  in Fig. 3(b). The forward current ( $j_{ext} > 0$ ) reduces  $h_v$  while the backward current ( $j_{ext} < 0$ ) enhances the  $h_v$  [inset in Fig. 3(b)]. SDE persists with two modified  $j_{c\pm}$  (dark green stars). When  $n = 510$  [Fig. 3(c)],  $h_v^0$  is relatively strong and the system enters a ‘strong’ helical superconducting phase as indicated by Figs. 2(c,d). The depairing currents  $\tilde{j}_{c\pm}$  are relatively small at  $j_{ext} = 0$ . Interestingly, since there is a

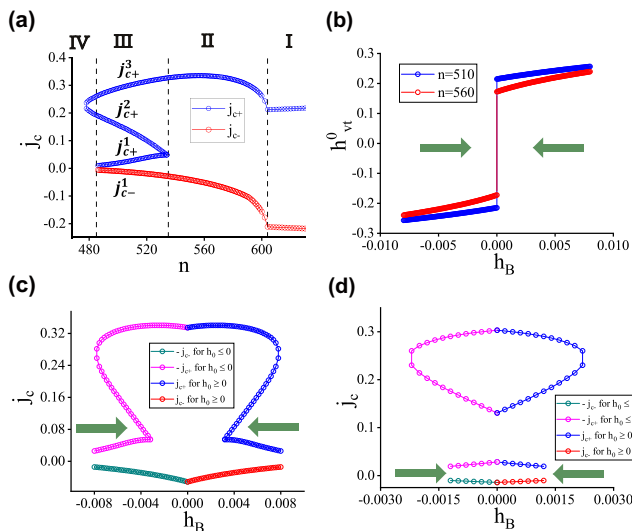


FIG. 4. (a) The variation of  $j_{c\pm}$  as a function of  $n$ . (b) The modulation of the total valley splitting field  $h_{vt}^0$  with  $h_B$  induced by the external magnetic field. (c,d)  $j_{c\pm}$  versus  $h_B$  for  $n = 560$  (c) and  $n = 510$  (d) [53]. The dark green arrows denote the scanning directions of the magnetic field  $B$  or  $h_B$ .

sudden change in the slope of curve  $\tilde{j}_{c+}(j_{ext})$  [as indicated in Fig. 2(e)], the number of intersection points could be four, which are symbolized by four actual critical currents ( $j_{c-}^1$  and  $j_{c+}^{1-3}$ ). Analogous to re-entrant superconductivity induced by applied magnetic fields [54, 55], We call this phenomenon as current-induced re-entrant superconductivity, regarding that there exist two different superconducting phases with two distinct critical current intervals. Once  $h_v^0$  becomes too large [see Fig. 3(d) with  $n = 480$ ],  $j_{c\pm}^1$  obviously shrink towards zero and hard to be measured in the experiment, while  $j_{c+}^{2,3}$  persist. Now it exhibits the extreme nonreciprocity only with two positive actual critical currents.

For clarity, we use colored dashed lines to mark normal phase regions (magenta) and superconducting regions (light blue) in Fig. 3. From the perspective of the free energy, at a definite applied current  $j_{ext}$  and the corresponding valley splitting field  $h_v(j_{ext})$ , the light blue regions and magenta regions indicate superconducting phases and normal phases carrying this current have a lower free energy, respectively. Considering our physical picture in Fig. 1(a) will be invalid in superconduct-

ing (light blue) regions, more rigorously, our theory is appropriate to describe a transition process from a normal phase (magenta) to a superconducting phase (light blue), as indicated by dark green arrows in Fig. 3. Different from previous theories, it means when the system is initially prepared in the normal phase and driven by the applied current to cross intersection points, the normal phase will be unstable and spontaneously enter the superconducting phase. However, a hysteresis behavior is likely to happen when the system in turn transitions from the superconducting phase to the normal phase. An illumination of this hysteresis requires a detailed investigation on the effect of supercurrents on valley polarizations in superconducting phase [37]. In total, our theory still gives a possible mechanism to remodulate the critical current intervals shown in Fig. 3(c) and extreme nonreciprocal SDE shown in Fig. 3(d). The latter also offers a possible explanation for the experimental observations in ref. [12].

### C. The variation of actual critical currents with different parameters

To study the SDE comprehensively, in Fig. 4(a) we extract  $j_{c\pm}$  based on the intersection points in Fig. 3 and show them in a wide range of electron occupations  $n$ . We here denote four regions. In region **I**, the system does not exhibit SDE due to zero  $h_v^0$ . In region **II**,  $h_v^0$  is moderate and the conventional SDE with  $j_{c+} \neq |j_{c-}|$  is observed.  $j_{c+} - |j_{c-}|$  becomes roughly larger as  $n$  decreases ( $h_v^0$  climbs). In region **III**,  $h_v^0$  is relatively large. The system exhibits re-entrant superconductivity with four actual critical currents ( $j_{c-}^1$  and  $j_{c+}^{1-3}$ ). In region **IV**,  $h_v^0$  is stronger and  $j_{c\pm}^1$  become too small to be observed. Only  $j_{c+}^{2,3}$  are left and the system exhibits an obvious extreme nonreciprocity. When  $h_v^0$  grows to too large ( $n$  is small), both  $j_{c+}^{2,3}$  will disappear and the superconducting phase cannot exist. In general, the extreme nonreciprocity occurs near the disappearance of superconductivity in our theory, which is akin the feature in ref [12].

Besides varying fillings, we also investigate how an external magnetic field  $B$  can modulate  $j_{c\pm}$ . Similar to the experiment [12], we consider the valley  $\tau$  locked with spin  $s_z$ , which is regarded from the Ising spin-orbit coupling [56, 57]. Thus,  $B$  can couple to valley through a Zeeman effect and induce an additional valley splitting field  $h_B \propto B$  into the Hamiltonian  $H_{MF}^v = \sum_{k,\tau} (E_{k,\tau} - h_B \tau) c_{k,\tau}^\dagger c_{k,\tau}$ . Through similar self-consistent calculations in Eq. (3), the total valley splitting field  $h_{vt}^0 = h_v^0 + h_B$  is refreshed along the magnetic field.

In Fig. 4(b), we plot the calculated  $h_{vt}^0$  versus  $h_B$ . Note that here the system is initially prepared at  $h_v^0 > 0$  ( $h_v^0 < 0$ ) before applying the magnetic field  $B > 0$  ( $B < 0$ ). It roughly reflects  $B$  scanned from positive

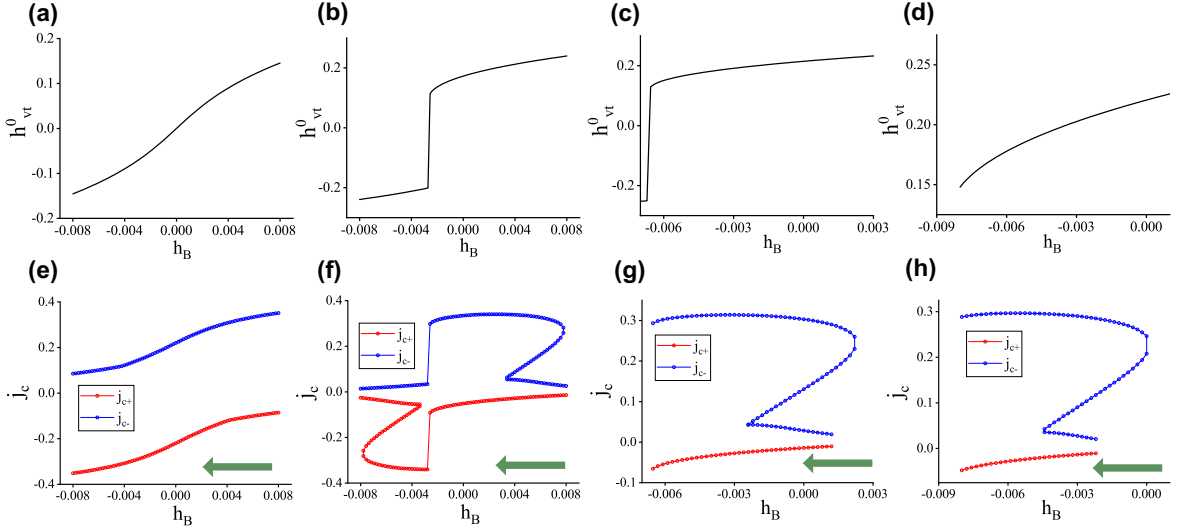


FIG. 5. (a-d) The change of the total valley splitting field  $h_{vt}^0$  as a function of the  $h_B$  for electron occupation  $n = 640$  (a),  $n = 560$  (b),  $n = 510$  (c) and  $n = 480$  (d). The system is initially prepared at the stable state at  $m \geq 0$  without the external magnetic field  $B$ . And the magnetic field as well as the additional valley splitting field  $h_B$  is scanned from positive to negative which influences the self-consistent result  $h_{vt}^0$  in every step. (e-h) the change of the actual critical currents  $j_c$  as a function of  $h_B$ , corresponding to the cases in (a-d), respectively. The dark green arrows denote the scanning direction.

(negative) direction to zero (see dark green arrows). Note that these two cases are antisymmetric due to TRS. And we can find  $|h_{vt}^0|$  decays as  $|h_B|$  weakens. We also plot  $j_c$  versus  $h_B$  for two distinct  $n$ . For  $n = 560$  in Fig. 4(c), as  $h_B$  sweeps from positive to zero, the decay of  $h_{vt}^0$  drives the number of actual critical currents from 4 to 2. Thus, the system evolves from a re-entrant superconducting phase to a conventional SDE. For  $n = 510$  in Fig. 4(d), the system becomes an extreme nonreciprocal SDE with two positive  $j_c$  at  $|h_B| \approx 0.002$ . The decline of  $|h_B|$  pulls down  $h_{vt}^0$  and impels the system into re-entrant superconducting phase with four distinct  $j_c$ .

Additionally, the polarity of SDE may be also reversed when scanning  $B$  from the positive to negative direction, see Fig. 5. At these cases, the system is initially prepared at  $m \geq 0$  for  $n = 640$  [Figs. 5(a,e)],  $n = 560$  [Figs. 5(b,f)],  $n = 510$  [Figs. 5(c,g)] and  $n = 480$  [Figs. 5(d,h)]. Then, we apply and scan  $h_B \propto B$  from positive to negative (dark green arrows). For  $n = 640$ , since no valley polarization appears without the external magnetic field ( $h_B = 0$ ), both the sign of  $h_{vt}^0$  and the polarity of SDE correlates well with  $h_B$  [Figs. 5(a,e)]. For the case of  $n = 560$  and  $n = 510$ , a sudden sign change of  $h_{vt}^0$  appears as  $h_B$  reaches about  $-0.0027$  [Fig. 5(b)] and  $-0.007$  [Fig. 5(c)], respectively. This switching could also reverse the polarity of SDE in Fig. 5(f). Note that the switching of  $h_{vt}^0$  in Fig. 5(c) is so large that  $j_{c\pm}$  disappears in Fig. 5(g). Similar to Fig. 4, the number of  $j_c$  also varies with  $h_B$  which manifests the transformation of types of SDE [Figs. 5(f,g)]. When the initial valley splitting field  $h_v^0$  without  $h_B$  is too large for  $n = 480$  ( $h_v^0 > 0.2$ ), a small variation of magnetic field is not enough to switch total valley splitting field  $h_{vt}^0$  [Fig. 5(d)]. But the super-

conducting phase gradually transforms from an extreme nonreciprocity with two positive  $j_c$  to the re-entrant superconductivity with four  $j_c$  and then to the conventional SDE with  $j_{c+} > 0, j_{c-} < 0$  [Fig. 5(h)].

In summary, our results in Fig. 4 and Fig. 5 both demonstrate that the extreme nonreciprocity can occur and be adjusted by the variation of the electron occupation  $n$  and the external magnetic field  $B$ . Additionally, our results are robust to changes in system size (see Appendix D).

## VI. DISCUSSIONS AND CONCLUSIONS

For better to compare with real situations, we can give a rough estimation on our calculated results. Considering a narrow bandwidth of the flat band with  $4t = 10$  meV [58–61], the energy unit is  $t = 2.5$  meV and the current unit is  $\frac{e}{h}t \approx 96.6$  nA. Thus, the set temperature  $T$  in the unit of Kelvin is around 2.9 K. In Fig. 2, the initial valley splitting field  $h_v^0$  varies from 0 to about  $0.2t$  (0.5 meV) and the maximal superconducting order parameter is  $\Delta \approx 0.33t \approx 0.83$  meV. In Fig. 4(a), we can roughly estimate the amplitudes of critical currents  $j_{c\pm}$  vary from 0 to 34 nA, which is in order of magnitude consistent with the previous experiment results [12]. It is also worth noting that the current in order of nA is experimentally confirmed to be able to affect the valley polarization in twisted bilayer graphene [38, 39], which reflects the reliability of our theoretical scheme. Totally speaking, the modulation of valley splitting field caused by the weak current is not strong in our results. See Fig. 3,  $h_v$  changes by about  $0.1t$  (about 0.25 meV) as the

current changes by about  $0.4\frac{e}{h}t$  (about 40 nA).

In conclusion, based on a simple valley-polarized model, we have revealed that depairing currents can be remodulated due to the current-induced valley polarization modulation. Depending on specific features, we have demonstrated that such a remodulation can induce the extreme nonreciprocity and also the current-induced re-entrant superconductivity. These special SDE can be further adjusted by varying electron occupations and external magnetic fields. Our study reflects the peculiarity in the interplay between valley ferromagnetism and superconductivity, provide a possible mechanism to explain experimental observations of extreme nonreciprocal SDE and open a new way to implement SDE with 100% efficiency.

### ACKNOWLEDGMENTS.

We thank Yue Mao, Yu-Hao Wan and Yi-Xin Dai for illuminating discussions. This work was financially supported by the National Natural Science Foundation of China (Grant No. 12374034 and No. 11921005), the National Key R and D Program of China (Grant No. 2024YFA1409002), and the Innovation Program for Quantum Science and Technology (2021ZD0302403) and the Postdoctoral Fellowship Program of CPS Funder Grant Number GZB20240031. We also acknowledge the High-performance Computing Platform of Peking University for providing computational resources.

### Appendix A: Formulations of the current-induced valley polarization modulation

When the applied current  $j_{ext}$  flows through the valley-polarized system shown in Eq. (1), occupations for electrons with opposite group velocities should be further imbalanced. In detail, taking a 1D system as an example with  $\mathcal{V} = Na$  where  $a = 1$  is the length unit, the Fermi level of electrons with positive (negative) velocities, coming from the source (drain) will rise (fall)  $\frac{eV}{2}$ , respectively. Then, the electron occupation  $n_\tau$  on each valley  $\tau$  changes into:

$$n_\tau = \sum_k f[\epsilon_{k,\tau} - \tilde{\mu} - h_v\tau - \frac{eV}{2}\text{sgn}(\epsilon'_{k,\tau})] \quad (\text{A1})$$

with  $\text{sgn}(x > 0) = 1$ ,  $\text{sgn}(x = 0) = 0$ ,  $\text{sgn}(x < 0) = -1$ . And  $e$  is the electron charge. For a small bias  $V \rightarrow 0$ , Eq. (A1) can be further approximated as:

$$n_\tau \approx n_\tau^0 - \frac{eV}{2} \sum_k \text{sgn}(\epsilon'_{k,\tau}) f'(\epsilon_{k,\tau} - \tilde{\mu} - h_v\tau), \quad (\text{A2})$$

where  $n_\tau^0 = \sum_k f(\epsilon_{k,\tau} - \tilde{\mu} - h_v\tau)$  is the original electron occupation before applying the current  $j_{ext}$ . Furthermore, the current  $j_{ext}$  flowing through the system which

is closely related to the voltage  $V$  can be also calculated:

$$\begin{aligned} j_{ext} &= \frac{e}{\hbar N} \sum_{k,\tau} \epsilon'_{k,\tau} f[\epsilon_{k,\tau} - \tilde{\mu} - h_v\tau - \frac{eV}{2}\text{sgn}(\epsilon'_{k,\tau})] \\ &\approx \frac{e}{\hbar} \int dk \sum_\tau \epsilon'_{k,\tau} f[\epsilon_{k,\tau} - \tilde{\mu} - h_v\tau - \frac{eV}{2}\text{sgn}(\epsilon'_{k,\tau})]. \end{aligned} \quad (\text{A3})$$

Here we regard the  $N \rightarrow \infty$  and thus the summation of  $k$  changes into the integral for simplicity. Similarly, when the bias is small with  $V \rightarrow 0$ , the current in Eq. (A3) can be approximated as:

$$j_{ext} \approx \frac{e^2 V}{\hbar} \sum_\tau [-f(\epsilon_{k,\tau}^{max} - \tilde{\mu} - h_v\tau) + f(\epsilon_{k,\tau}^{min} - \tilde{\mu} - h_v\tau)], \quad (\text{A4})$$

where  $\epsilon_{k,\tau}^{max}$  and  $\epsilon_{k,\tau}^{min}$  is the global maximum and minimum value of  $\epsilon_{k,\tau}$ . For a low temperature  $T \rightarrow 0$  and  $\tilde{\mu} \in (\epsilon_{k,\tau}^{min} - h_v\tau, \epsilon_{k,\tau}^{max} - h_v\tau)$ ,  $j_{ext} = \frac{2e^2 V}{\hbar}$  well corresponds to Landauer-Büttiker formula in a ballistic regime [48]. Substituting Eq. (A4) into Eq. (A2), we can get the relation between  $n_\tau$  and  $j_{ext}$  as

$$n_\tau = n_\tau^0 + \alpha_\tau j_{ext}, \quad (\text{A5})$$

and also the change of valley splitting field  $h_v$ :

$$h_v = \frac{U_v}{2\mathcal{V}}(n_+ - n_-) = \frac{U_v}{2\mathcal{V}}(\alpha_+ - \alpha_-)j_{ext} + h_v^0 \quad (\text{A6})$$

where  $h_v^0$  is the initial valley splitting field when  $j_{ext} = 0$ . The Eq. (A6) is just Eq. (3) in the main text. The coefficient  $\alpha_\tau$  to measure the ability for the current to modulate the valley polarization is a function of modified chemical potential  $\tilde{\mu}$  and valley splitting field  $h_v$ :

$$\begin{aligned} \alpha_\tau(\tilde{\mu}, h_v) &= \frac{\hbar \sum_k \text{sgn}(\epsilon'_{k,\tau}) f'(\epsilon_{k,\tau} - \tilde{\mu} - h_v\tau)}{2e \sum_\tau [f(\epsilon_{k,\tau}^{max} - \tilde{\mu} - h_v\tau) - f(\epsilon_{k,\tau}^{min} - \tilde{\mu} - h_v\tau)]}. \end{aligned} \quad (\text{A7})$$

During applying an electric current  $j_{ext}$ , the change of  $h_v$  and  $\tilde{\mu}$  could alter the value of  $\alpha_\tau$  in time. For simplicity, we ignore this effect and directly set  $\alpha_\tau(\tilde{\mu}, h_v)$  as  $\alpha_\tau(\tilde{\mu}^0, h_v^0)$ .

Especially when  $T \rightarrow 0$ ,  $\alpha_\tau \propto \sum_n \frac{1}{\epsilon'_\tau(k_F^n)}$  where  $k_F^n$  is the  $n$ -th Fermi wave vector at the Fermi level  $E_f$ . Thus, the value of  $\alpha_\tau$  is closely related to the inverse of Fermi velocities  $v_F^n = \frac{1}{\hbar} \epsilon'_\tau(k_F^n)$ . If the energy band has the intravalley inversion symmetry:  $\epsilon_{k,\tau} = \epsilon_{-k,\tau}$ . It leads to  $\epsilon'_{k,\tau} = -\epsilon'_{-k,\tau}$  and  $\alpha_\tau$  as well as the change in Eq. (A6) should be canceled to be zero. The necessity of intravalley inversion breaking is consistent with the finding in ref. [40]. In addition, the intravalley inversion symmetry breaking is also found as a crucial condition to realize the SDE in the valley polarized system [49]. This coincidence implies the possibility for the combination between the current-induced valley polarization modulation and SDE.



In numerical calculations, we do not directly use the  $\alpha_\tau$  to obtain the results of current-induced valley modulation in Eq. (A6). To be more accurate, after given the applied current  $I_{ext}$ , we use Eq. (A4) to obtain the corresponding bias energy  $eV$ . Then we bring  $eV$  into Eq. (A1) to get the electron occupation  $n_\tau$  on each valley and also use  $h_v = \frac{U_v}{2V}(n_+ - n_-)$  to obtain the corresponding  $h_v$ . Note that the modified chemical potential  $\tilde{\mu}$  and the valley splitting field  $h_v$  are fixed as  $\tilde{\mu}^0$  and  $h_v^0$  in the right parts in Eq. (A1)–Eq. (A4). In Eq. (A1), we do not assume that the bias  $eV$  is small, so that  $h_v = \frac{U_v}{2V}(n_+ - n_-)$  versus the bias  $eV$  deviates slightly from the linear relation (see the insets of Fig. 3).

### Appendix B: The self-consistent manner including the effect of applied currents

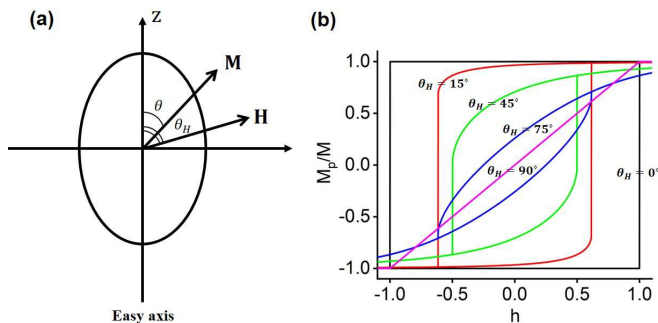


FIG. 6. (a) The model for a single-domain spheroidal particle endowed with uniaxial magnetic anisotropy. The magnetization  $\mathbf{M}$  is aligned with an angle  $\theta$  between the easy axis  $z$  and the external magnetic field  $\mathbf{H}$  is aligned with an angle  $\theta_H$  between the easy axis  $z$ . (b) The numerical calculated magnetization curves between  $M_p/M$  and  $h$  for different angles  $\theta_H$ .

In the main text, we set the total valley polarization in Eq. (5) is the summation of the current-induced part and the spontaneous polarization part from the Coulomb interaction. The influence on  $h_v^0$  by the applied current  $j_{ext}$  is just neglected. In this Appendix, we will discuss this self-consistent process theoretically and demonstrate the rationality of our linear approximation in Eq. (5) for a small  $j_{ext}$ .

Actually, Eq. (5) is easy to recall from the relationship between the magnetic induction  $\mathbf{B}$  and magnetic field strength  $\mathbf{H}$ :

$$\mathbf{B}/\mu_0 = \mathbf{M} + \mathbf{H}. \quad (\text{B1})$$

where  $\mathbf{M}$  is the magnetization and  $\mu_0$  is the permeability of free space. Neglecting the coefficients,  $j_{ext}$ ,  $h_v^0$  and  $h_v$  in Eq. (5) just corresponds to  $\mathbf{H}$ ,  $\mathbf{M}$  and  $\mathbf{B}$  in Eq. (B1), respectively. In the magnetization process, the external magnetic field strength  $\mathbf{H}$  could also affect the intrinsic magnetization  $\mathbf{M}(\mathbf{H})$ , causing the relationship between  $\mathbf{B}$  and  $\mathbf{H}$  more complicated, usually along with magnetic

hysteresis loops. Based on a rough analogy, we can draw on the magnetic curve of  $M = F(H)$  to further speculate the behaviors of  $h_v^0 = F(I_{ext})$ .

Strictly speaking, spin and valley cannot be simply equivalent, considering there are some differences between them. Thus, the analogy between valley and spin is just a crude mean to help understanding. However, since valley and spin also have some similarities in our model, this analogy is still plausible to some extent. At first, our theory is simply built on a two-band Stoner Hamiltonian where valley only serves as a flavor degree of the energy bands. In principle, replacing the valley index with the spin index has no intrinsic influence on our theoretical analysis and the physical picture in Fig. 1. In some previous studies in graphene systems, the polarization of spin and valley flavors is often regarded as isospin magnetism as a whole [45, 46]. Secondly, the spin and valley are found to be locked together due to the presence of proximity-induced Ising SOC [12], which also indicates the effect of valley and spin has some equivalence in the experiment.

In the following part, we will explain the influence on  $h_v^0$  by  $j_{ext}$  based on two fashioned theoretical perspectives: Stoner-Wohlfarth model and Rayleigh law.

**To analyze the function of  $h_v^0 = F(I_{ext})$  from Stoner-Wohlfarth model.** The theory of Stoner-Wohlfarth model is based on the coherent rotation of the magnetization in a single-domain particle [62]. This is a simple theoretical model, but it could illustrate the rationality of our approximation to some extent. As shown in Fig. 6 (a), a spheroidal single-domain particle endowed with uniaxial anisotropy. The magnetization  $\mathbf{M}$  is aligned with an angle  $\theta$  between the easy axis. The internal energy density is expressed as a function of  $\theta$  as [63]:

$$u_{an}(\theta) = K_u \sin^2(\theta). \quad (\text{B2})$$

Here  $K_u$  is the anisotropy parameter which is related to the magnetocrystalline anisotropy and shape effects. Then we consider the single domain subjected an applied magnetic field  $\mathbf{H}$  making the angle  $\theta_H$  with the easy axis, and the field interaction energy density is [63]:

$$u_H(\theta) = -\mu_0 M H \cos(\theta_H - \theta). \quad (\text{B3})$$

Thus, the total Gibbs free energy density is:

$$g(\theta) = u_{an}(\theta) + u_H(\theta) = K_u \sin^2(\theta) - \mu_0 M H \cos(\theta_H - \theta). \quad (\text{B4})$$

Note that here we only pay attention on the coherent rotation of  $\mathbf{M}$  with the strength of  $\mathbf{M}$  unchanged. And the value of  $\mathbf{H}$  oscillating between positive and negative values with  $\theta_H$  varying between  $0^\circ$  and  $90^\circ$ . The equilibrium conditions are obtained as  $g(\theta)$  reaches the minimum. For convenience, we reduce the  $g(\theta)$  as

$\tilde{g}(\theta) = g(\theta)/(2K_u)$ . The equilibrium conditions are:

$$\frac{d\tilde{g}}{d\theta} = \frac{1}{2}\sin(2\theta) - h\sin(\theta_H - \theta) = 0 \quad (\text{B5a})$$

$$\frac{d^2\tilde{g}}{d^2\theta} = \cos(2\theta) + h\cos(\theta_H - \theta) > 0. \quad (\text{B5b})$$

where  $h = \mu_0 MH/2K_u = H/H_K$ . The solution of Eq. (B5) can be studied analytically in some cases. For example, when  $\theta_H = 0$ , the magnetic field  $\mathbf{H}$  is aligned with the easy axis, and the solution of Eq. (B5a) is  $\sin(\theta) = 0$  and  $\cos(\theta) = -h$ . For the first case,  $\theta = 0, \pi$  and Eq. (B5b) gives  $\frac{d^2\tilde{g}}{d^2\theta} = 1 \pm h > 0$ . For the second case,  $\theta = \arccos(-h)$  and Eq. (B5b) gives  $\frac{d^2\tilde{g}}{d^2\theta} = h^2 - 1 > 0$ . In general,  $h < -1, \theta = \pi$ ;  $h > 1, \theta = 0$ ;  $-1 \leq h \leq 1, \theta = 0$  or  $\pi$  (depending on the initial path). To further demonstrate, we plot the magnetization resolved in the field direction  $M_p(\theta_H) = M\cos(\theta_H - \theta)$  under the cyclic variation of the field  $h = H/H_K$  in Fig. 6(b) with  $\theta_H = 0^\circ, 15^\circ, 45^\circ, 75^\circ, 90^\circ$ . The Fig. 6(b) is numerically calculated from Eq. (B5). It can be found that a change in  $h$  causes hysteresis loops where  $M_p$  can be reversed at certain critical value  $h_c$  (i.e. the coercive field). The characteristics of hysteresis loops are strongly dependent on the aligned angle  $\theta_H$  of  $\mathbf{H}$ . For  $\theta_H = 0$ , we can find a square hysteresis loop with  $M_p = \pm M$  [see the black solid line in Fig. 6(b)]. For the larger  $\theta_H$ , the hysteresis loop shrinks and finally becomes a linear function at  $\theta_H = 90^\circ$  [see the magenta solid line in Fig. 6(b)]. For an isotropic system of randomly oriented identical particles, the overall mean behaviour stems from an averaged hysteresis loop for different angles.

Next, we refer to the  $M_p = F(H)$  of the Stoner-Wohlfarth model shown in Fig. 6(b), and analyze the relationship  $h_v^0 = F(I_{ext})$ . There is a difference between the valley-polarization and the magnetization in ferromagnets. For the latter, a spin-rotation symmetry is maintained and the ferromagnetism is described by a vector order parameter. In contrast, the valley polarization in our system is Ising-like and not a vector [41]. The system is either polarized at  $K$  valley or  $K'$  valley, but never polarized at a valley-coherence state like  $\frac{1}{\sqrt{2}}(|K\rangle + |K'\rangle)$ . This means the direction of the valley polarization is only aligned along the easy axis ( $z$  axis). In addition, since the applied current  $I_{ext}$  will influence the valley polarization but cannot mix two valleys, the effect of  $I_{ext}$  should be analogous to the effect of  $\mathbf{H}$  at  $\theta_H = 0^\circ$ . Therefore, the curve of  $h_v^0(I_{ext})$  should be similar to the curve of  $M_p(H)$  at  $\theta_H = 0^\circ$  as shown by black solid lines in Fig. 6 (b) in a small single-domain valley-polarized system. Actually, even if in a multi-domain system, the averaged hysteresis loop could be still like the curve at  $\theta_H = 0^\circ$ , because the easy axis of each domain is along the  $z$  direction. Therefore, we can conclude that  $h_v^0$  remains nearly unchanged as long as  $I_{ext}$  is not too large. Considering the current to flip the valley polarization sometimes demands to reach several tens of nA [38], which is basically larger than the

critical currents obtained by our numerical calculations, our linear approximation in Eq. (5) has some rationality.

**To analyze the function of  $h_v^0 = F(I_{ext})$  from the Rayleigh law.** For a further comparison, we next refer to another theory called as Rayleigh law, which is used to describe the behavior of ferromagnetic materials at low fields [64, 65]. The Rayleigh law is a technical model describing the magnetic hysteresis phenomenon with simple mathematical functions. It quantizes the initial magnetization curve as a second order equation [66]:

$$B(H) = aH + bH^2. \quad (\text{B6})$$

Here  $a$  corresponds to reversible part of the magnetization process with  $a = \lim_{H \rightarrow 0} \frac{\partial B}{\partial H} = \mu_0 \mu_i$  ( $\mu_i$  is the initial permeability), and  $b$  corresponds to the irreversible part of the magnetization process. Based on this initial magnetization curve, Rayleigh law describes the magnetic hysteresis loop by two symmetrical, intersecting parabolic curves [66]:

$$B(H) = (a + bH_m)H \pm \frac{b}{2}(H_m^2 - H^2). \quad (\text{B7})$$

Note that this function describes the behavior of magnetic induction  $B$  with the magnetic field  $H$ .  $H_m$  is the amplitude of the scanning magnetic field during the magnetization process. The '+' sign denotes the upper branch of the loop, while the '-' sign denotes the lower branch of the loop. We can draw an analogy from Eqs. (B6, B7), and give the initial valley polarization curve and the hysteresis for  $h_v$  as a function of the applied current  $j_{ext}$ , respectively:

$$h_v(j_{ext}) = aj_{ext} + bj_{ext}^2 \quad (\text{B8a})$$

$$h_v(j_{ext}) = (a + bj_{ext,m})j_{ext} \pm \frac{b}{2}(j_{ext,m}^2 - j_{ext}^2). \quad (\text{B8b})$$

Similarly,  $j_{ext,m}$  is the amplitude of scanning current, i.e. Eq. (B8b) is valid when  $|j_{ext}| \leq j_{ext,m}$ . Once  $j_{ext,m}$  is fixed, the form of  $h_v(j_{ext})$  is determined by the parameter  $a$  and  $b$ .

In general, the value of  $a$  and  $b$  can be obtained by experimental fittings. Here, we try to estimate them theoretically. According to Eq. (B6), the parameter  $a$  reflects the reversible part of the initial magnetization curve, which shows the relationship between  $H$  and  $M$  as the field strength is increased from a demagnetized magnet ( $H = M = 0$ ). To simulate this curve in a valley-polarized system, we use such an expression:

$$h_v = \frac{U_v}{4V} \sum_{k,\tau,\tau'} \tau f(\epsilon_{k,\tau} - \tilde{\mu}^0 - \frac{eV}{2} \text{sgn}(\epsilon'_{k,\tau}) - h_v^0 \tau \tau'). \quad (\text{B9})$$

Here  $\tau' = \pm$ . Actually, this expression is an average of the initial positive valley polarization  $h_v^0$  state and initial negative valley polarization  $-h_v^0$  state, which can be used

to simulate a demagnetized state. When the current is absent ( $eV = 0$ ),  $h_v$  can be evaluated to be zero. In detail, the parameter  $a$  is evaluated as:

$$\begin{aligned}
a &= \left. \frac{\partial h_v}{\partial I_{ext}} \right|_{I_{ext}=0} = \left. \frac{\partial h_v}{\partial eV} \right|_{eV=0} \left. \frac{\partial eV}{\partial I_{ext}} \right|_{I_{ext}=0} \\
&= -\frac{U_v}{4\mathcal{V}} \sum_{k,\tau} \tau f(\epsilon_{k,\tau} - \tilde{\mu}^0 - h_v^0 \tau) \frac{\text{sgn}(\epsilon'_{k,\tau})}{2} \gamma \\
&\quad - \frac{U_v}{4\mathcal{V}} \sum_{k,\tau} \tau f(\epsilon_{k,\tau} - \tilde{\mu}^0 + h_v^0 \tau) \frac{\text{sgn}(\epsilon'_{k,\tau})}{2} \gamma \\
&= -\frac{U_v}{4\mathcal{V}} \sum_{k,\tau} \tau f(\epsilon_{k,\tau} - \tilde{\mu}^0 - h_v^0 \tau) \frac{\text{sgn}(\epsilon'_{k,\tau})}{2} \gamma \\
&\quad - \frac{U_v}{4\mathcal{V}} \sum_{-k,-\tau} (-\tau) f(\epsilon_{-k,-\tau} - \tilde{\mu}^0 + (-\tau) h_v^0) \frac{\text{sgn}(\epsilon'_{-k,-\tau})}{2} \gamma \\
&= -\frac{U_v}{4\mathcal{V}} \sum_{k,\tau} \tau f(\epsilon_{k,\tau} - \tilde{\mu}^0 - h_v^0 \tau) \text{sgn}(\epsilon'_{k,\tau}) \gamma.
\end{aligned} \tag{B10}$$

Here we use the relation:  $\epsilon_{k,\tau} = \epsilon_{-k,-\tau}$  and  $\epsilon'_{k,\tau} = -\epsilon'_{-k,-\tau}$ . Referring to our derivation of Eq. (A4), the parameter  $\gamma$  is:

$$\begin{aligned}
\gamma &= \left. \frac{\partial eV}{\partial j_{ext}} \right|_{j_{ext}=0} \\
&\approx \frac{\hbar}{e} \sum_{\tau} [-f(\epsilon_{k,\tau}^{max} - \tilde{\mu}^0 - h_v^0 \tau) + f(\epsilon_{k,\tau}^{min} - \tilde{\mu}^0 - h_v^0 \tau)]^{-1}.
\end{aligned} \tag{B11}$$

Substituting Eq. (B11) into Eq. (B10), we can find the value of  $a$  is just equal to the value of  $\frac{U_v}{2\mathcal{V}}(\alpha_+ - \alpha_-)$  as shown in Eq. (A7), in view of  $\tilde{\mu} = \tilde{\mu}^0$  and  $h_v = h_v^0$  at  $j_{ext} = 0$  ( $eV = 0$ ). For the parameter  $b$ , it is related to the irreversible part of the initial magnetization curve and cannot be evaluated easily. However, we can assume a case for soft materials where the coercive field  $j_{ext}^c$  is very small [62]. The coercive field  $j_{ext}^c$  is the zero point of the function  $h_v(j_{ext})$ , satisfying  $(a + b j_{ext,m}) j_{ext}^c \pm \frac{b}{2} (j_{ext,m}^2 - (j_{ext}^c)^2) = 0$ . We take the case for '+' as an example (the case for '-' is similar) and get:

$$j_{ext}^c = \frac{(a + b j_{ext,m}) - a \sqrt{1 + 2 \frac{b}{a} j_{ext,m} + 2 \frac{b^2}{a^2} j_{ext,m}^2}}{b}. \tag{B12}$$

By using the condition of soft materials ( $|j_{ext}^c|$  is small), we deduce that  $\frac{b}{a} j_{ext,m} \ll 1$  from Eq. (B12). Therefore, in the case of soft materials,  $a \gg b j_{ext,m}$ , and Eq. (B8b) can be simplified as:  $h_v(j_{ext}) = a j_{ext} \pm \frac{b}{2} j_{ext,m}^2 = a j_{ext} \pm h_v^0$ . This corresponds to the linear relation shown in Eq. (5) in the main text.

Additionally, even if we expand the function in Eq. (B9) into the second order of  $I_{ext}$ , we can find the

expansion coefficient:

$$\begin{aligned}
\tilde{b} &\equiv \left. \frac{\partial^2 h_v}{\partial^2 j_{ext}} \right|_{j_{ext}=0} = \left. \frac{\partial^2 h_v}{\partial^2 eV} \gamma^2 \right|_{eV=0} \\
&= \frac{U_v \gamma^2}{16\mathcal{V}} \sum_{k,\tau} \tau f''(\epsilon_{k,\tau} - \tilde{\mu}^0 - h_v^0 \tau) \\
&\quad + \frac{U_v \gamma^2}{16\mathcal{V}} \sum_{k,\tau} \tau f''(\epsilon_{k,\tau} - \tilde{\mu}^0 + h_v^0 \tau) \\
&= 0.
\end{aligned} \tag{B13}$$

Although not rigorously, Eq. (B13) implies that the coefficient  $b$  is small at the bias  $eV = 0$ . This is some justification to assume  $b I_{ext,m} \ll a$  in our case.

In summary, from two fashioned theoretical perspectives, we demonstrate that the linear approximation between  $h_v$  and  $j_{ext}$  in Eq. (5) is still plausible when  $j_{ext}$  is relatively small, even though the effect of current or voltage is taken into account in the self-consistent process. Once  $j_{ext}$  becomes too large, the weak equilibrium of valley-dependent electron occupations can indeed be broken, and the total valley polarization will be reversed by the flowing current. But in principle, as long as the intersection points shown in Fig. 3 exist before valley flip happens, our physical pictures are still qualitatively valid.

### Appendix C: The effect of the band asymmetry

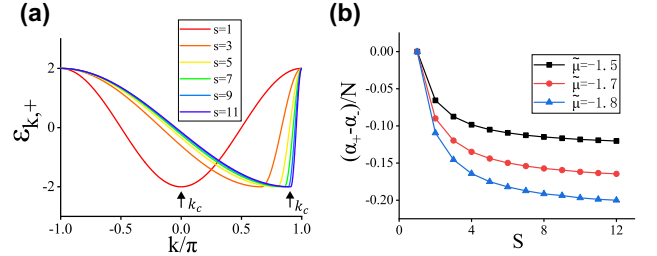


FIG. 7. (a) A series of  $K$  bands with distinct band asymmetries characterized by  $s$ . The  $K'$  bands are just their TRS counterparts and not shown here.  $k_c$  denotes the position of the local minimum for the energy band. (b) the change of coefficient  $(\alpha_+ - \alpha_-)/N$  as a function of  $s$  for different  $\tilde{\mu}$  with  $h_v^0 = 0.1$ .

As stated in Fig. 1, the key factor to realize the extreme nonreciprocity is the coefficient  $\alpha_+ - \alpha_-$  which measures the ability of the applied current  $j_{ext}$  to modulate the valley polarization. As proved in Appendix A,  $\alpha_\tau$  strongly depends the band asymmetry. So in Fig. 7, we investigate how the band asymmetry affects the coefficient  $\alpha_+ - \alpha_-$ . In Fig. 7(a), a series of 1D  $K$  valley bands are considered:  $\epsilon_{k,+} = -2t \cos[\frac{s}{2s-1}(k - \frac{s-1}{s}\pi)]$  for  $-\pi \leq k \leq \frac{(s-1)}{s}\pi$  and  $\epsilon_{k,+} = -2t \cos(sk - \pi) * (-1)^s$

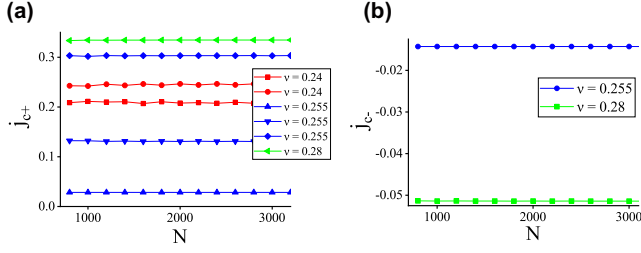


FIG. 8. (a,b) the change of  $j_{c+}$  (a) and  $j_{c-}$  (b) as a function of the system size  $N$  for the fixed proportion of the number of electrons  $v = 0.24, 0.255, 0.28$ .

for  $\frac{(s-1)}{s}\pi < k < \pi$ . Note that  $\epsilon_{k,-} = \epsilon_{-k,+}$ . Here  $s$  is introduced to denote the location of the wavevector for the global minimum  $k_c = \frac{s-1}{s}\pi$  [see Fig. 7(a)]. As  $s$  increases from 1,  $k_c$  tends to be close to  $\pi$  and the energy band  $\epsilon_{k,\tau}$  becomes more asymmetric. For the calculations in the main text,  $s$  is set as 8. In Fig. 7(b), under an fixed initial valley splitting field  $h_v^0 = 0.1$ , the magnitude of  $(\alpha_+ - \alpha_-)/N$  shows an apparent tendency to grow as  $s$  climbs, see Fig. 7(b) for three different  $\tilde{\mu}$ . Since a larger coefficient  $\alpha_+ - \alpha_-$  implies the current  $j_{ext}$  can weaken the valley polarization  $h_v$  faster, more asymmetric energy bands are more likely to induce the extreme

nonreciprocity.

#### Appendix D: The convergence of results for the system size

In principle, as long as the proportion of the number of electrons (the filling factor)  $v = n/N$  in the system is fixed, our conclusions in the main text should remain unchanged as  $N \rightarrow \infty$ . To confirm our calculations have converged, we increase the system size  $Na$  ( $a = 1$ ) by fixing  $v = 0.24, 0.255, 0.28$  respectively. The changes of actual critical current  $j_{c+}$  and  $j_{c-}$  as a function of  $N$  are shown in Fig. 8, respectively. Actually,  $v = 0.24$  corresponds to  $n = 480$  when  $N = 2000$  [Fig. 3(d)] where the system enters an extreme nonreciprocity only with two positive  $j_{c+}$  [red lines in Fig. 8(a)].  $v = 0.255$  corresponds to  $n = 510$  with  $N = 2000$  [Fig. 3(c)] and the system enters the re-entrant superconductivity with four distinct critical currents  $j_c$  [dark blue lines in Figs. 8(a,b)].  $v = 0.28$  corresponds to  $n = 560$  with  $N = 2000$  [Fig. 3(b)] where the system enters the conventional SDE with  $j_{c+} > 0$  and  $j_{c-} < 0$  [light green lines in Fig. 8]. Fig. 8 clearly indicate actual critical currents  $j_c$  remain nearly unchanged as the system size  $N$  varies from 800 to 3200.

- 
- [1] M. Nadeem, M. S. Fuhrer, and X. Wang, The superconducting diode effect, *Nat. Rev. Phys.* **5**, 558 (2023).
- [2] K. Jiang and J. Hu, Superconducting diode effects, *Nat. Phys.* **18**, 1145 (2022).
- [3] A. I. Braginski, Superconductor electronics: status and outlook, *J. Supercond. Nov. Magn.* **32**, 45 (2019).
- [4] J. Linder and J. W. A. Robinson, Superconducting spintronics, *Nat. Phys.* **11**, 307 (2015).
- [5] G. Wendin, Quantum information processing with superconducting circuits: a review, *Rep. Prog. Phys.* **80**, 106001 (2017).
- [6] X. Liu and M. C. Hersam, 2D materials for quantum information science, *Nat. Rev. Mater.* **4**, 669 (2019).
- [7] F. Ando, Y. Miyasaka, T. Li, J. Ishizuka, T. Arakawa, Y. Shiota, T. Moriyama, Y. Yanase, and T. Ono, Observation of superconducting diode effect, *Nature (London)* **584**, 373 (2020).
- [8] Y. Miyasaka, R. Kawarazaki, H. Narita, F. Ando, Y. Ikeda, R. Hisatomi, A. Daido, Y. Shiota, T. Moriyama, Y. Yanase, and T. Ono, Observation of nonreciprocal superconducting critical field, *Appl. Phys. Express* **14**, 073003 (2021).
- [9] Y. M. Itahashi, T. Ideue, Y. Saito, S. Shimizu, T. Ouchi, T. Nojima, and Y. Iwasa, Nonreciprocal transport in gate-induced polar superconductor SrTiO<sub>3</sub>, *Sci. Adv.* **6**, eaay9120 (2020).
- [10] H. Narita, J. Ishizuka, R. Kawarazaki, D. Kan, Y. Shiota, T. Moriyama, Y. Shimakawa, A. V. Ognev, A. S. Samardak, Y. Yanase, and T. Ono, Field-free superconducting diode effect in noncentrosymmetric superconductor/ferromagnet multilayers, *Nat. Nanotechnol.* **17**, 823 (2022).
- [11] M. Masuko, M. Kawamura, R. Yoshimi, M. Hirayama, Y. Ikeda, R. Watanabe, J. J. He, D. Maryenko, A. Tsukazaki, K. S. Takahashi, M. Kawasaki, N. Nagao, and Y. Tokura, Nonreciprocal charge transport in topological superconductor candidate Bi<sub>2</sub>Te<sub>3</sub>/PdTe<sub>2</sub> heterostructure, *npj Quantum Mater.* **7**, 104 (2022).
- [12] J.-X. Lin, P. Siriviboon, H. D. Scammell, S. Liu, D. Rhodes, K. Watanabe, T. Taniguchi, J. Hone, M. S. Scheurer, and J. I. A. Li, Zero-field superconducting diode effect in small-twist-angle trilayer graphene, *Nat. Phys.* **18**, 1221 (2022).
- [13] L. Bauriedl, C. Bäuml, L. Fuchs, C. Baumgartner, N. Paulik, J. M. Bauer, K.-Q. Lin, J. M. Lupton, T. Taniguchi, K. Watanabe, C. Strunk, and N. Paradiso, Supercurrent diode effect and magnetochiral anisotropy in few-layer NbSe<sub>2</sub>, *Nat. Commun.* **13**, 4266 (2022).
- [14] C. Baumgartner, L. Fuchs, A. Costa, S. Reinhardt, S. Gronin, G. C. Gardner, T. Lindemann, M. J. Manfra, P. E. Faria Junior, D. Kochan, J. Fabian, N. Paradiso, and C. Strunk, Supercurrent rectification and magnetochiral effects in symmetric Josephson junctions, *Nat. Nanotechnol.* **17**, 39 (2022).
- [15] K.-R. Jeon, J.-K. Kim, J. Yoon, J.-C. Jeon, H. Han, A. Cottet, T. Kontos, and S. S. P. Parkin, Zero-field polarity-reversible Josephson supercurrent diodes enabled by a proximity-magnetized Pt barrier, *Nat. Mater.* **21**, 1008 (2022).
- [16] H. Wu, Y. Wang, Y. Xu, P. K. Sivakumar, C. Pasco, U. Filippozzi, S. S. P. Parkin, Y.-J. Zeng, T. McQueen, and M. N. Ali, The field-free Josephson diode in a van der

- waals heterostructure, *Nature (London)* **604**, 653 (2022).
- [17] B. Pal, A. Chakraborty, P. K. Sivakumar, M. Davydova, A. K. Gopi, A. K. Pandeya, J. A. Krieger, Y. Zhang, M. Date, S. Ju, N. Yuan, N. B. M. Schröter, L. Fu, and S. S. P. Parkin, Josephson diode effect from Cooper pair momentum in a topological semimetal, *Nat. Phys.* **18**, 1228 (2022).
- [18] F. K. de Vries, E. Portolés, G. Zheng, T. Taniguchi, K. Watanabe, T. Ihn, K. Ensslin, and P. Rickhaus, Gate-defined Josephson junctions in magic-angle twisted bilayer graphene, *Nat. Nanotechnol.* **16**, 760 (2021).
- [19] J. Díez-Mérida, A. Díez-Carlón, S. Y. Yang, Y. M. Xie, X. J. Gao, J. Senior, K. Watanabe, T. Taniguchi, X. Lu, A. P. Higginbotham, K. T. Law, and D. K. Efetov, Symmetry-broken Josephson junctions and superconducting diodes in magic-angle twisted bilayer graphene, *Nat. Commun.* **14**, 2396 (2023).
- [20] B. Turini, S. Salimian, M. Carrega, A. Iorio, E. Strambini, F. Giazotto, V. Zannier, L. Sorba, and S. Heun, Josephson diode effect in high-mobility InSb nanoflags, *Nano Lett* **22**, 8502 (2022).
- [21] M. Trahms, L. Melischek, J. F. Steiner, B. Mahendru, I. Tamir, N. Bogdanoff, O. Peters, G. Reecht, C. B. Winkelmann, F. von Oppen, and K. J. Franke, Diode effect in Josephson junctions with a single magnetic atom, *Nature (London)* **615**, 628 (2023).
- [22] Y.-Y. Lyu, J. Jiang, Y.-L. Wang, Z.-L. Xiao, S. Dong, Q.-H. Chen, M. V. Milošević, H. Wang, R. Divan, J. E. Pearson, P. Wu, F. M. Peeters, and W.-K. Kwok, Superconducting diode effect via conformal-mapped nanoholes, *Nat. Commun.* **12**, 2703 (2021).
- [23] E. Strambini, M. Spies, N. Ligato, S. Ilić, M. Rouco, C. González-Orellana, M. Ilyn, C. Rogero, F. S. Bergeret, J. S. Moodera, P. Virtanen, T. T. Heikkilä, and F. Giazotto, Superconducting spintronic tunnel diode, *Nat. Commun.* **13**, 2431 (2022).
- [24] G. L. J. A. Rikken, J. Fölling, and P. Wyder, Electrical magnetochiral anisotropy, *Phys. Rev. Lett.* **87**, 236602 (2001).
- [25] G. L. J. A. Rikken and P. Wyder, Magnetoelectric anisotropy in diffusive transport, *Phys. Rev. Lett.* **94**, 016601 (2005).
- [26] R. Wakatsuki and N. Nagaosa, Nonreciprocal current in noncentrosymmetric Rashba superconductors, *Phys. Rev. Lett.* **121**, 026601 (2018).
- [27] R. Wakatsuki, Y. Saito, S. Hoshino, Y. M. Itahashi, T. Ideue, M. Ezawa, Y. Iwasa, and N. Nagaosa, Nonreciprocal charge transport in noncentrosymmetric superconductors, *Sci. Adv.* **3**, e1602390 (2017).
- [28] J. J. He, Y. Tanaka, and N. Nagaosa, A phenomenological theory of superconductor diodes, *New. J. Phys.* **24**, 053014 (2022).
- [29] V. Barzykin and L. P. Gor'kov, Inhomogeneous stripe phase revisited for surface superconductivity, *Phys. Rev. Lett.* **89**, 227002 (2002).
- [30] K. Michaeli, A. C. Potter, and P. A. Lee, Superconducting and ferromagnetic phases in SrTiO<sub>3</sub>/LaAlO<sub>3</sub> oxide interface structures: Possibility of finite momentum pairing, *Phys. Rev. Lett.* **108**, 117003 (2012).
- [31] N. F. Q. Yuan and L. Fu, Topological metals and finite-momentum superconductors, *Proc. Natl Acad. Sci. USA* **118**, e2019063118 (2021).
- [32] H. D. Scammell, J. I. A. Li, and M. S. Scheurer, Theory of zero-field superconducting diode effect in twisted trilayer graphene, *2D Mater.* **9** (2022).
- [33] A. Daido, Y. Ikeda, and Y. Yanase, Intrinsic superconducting diode effect, *Phys. Rev. Lett.* **128**, 037001 (2022).
- [34] N. F. Q. Yuan and L. Fu, Supercurrent diode effect and finite-momentum superconductors, *Proc. Natl Acad. Sci. USA* **119**, e2119548119 (2022).
- [35] S. Ilić and F. S. Bergeret, Theory of the supercurrent diode effect in Rashba superconductors with arbitrary disorder, *Phys. Rev. Lett.* **128**, 177001 (2022).
- [36] A. Daido and Y. Yanase, Unidirectional superconductivity and diode effect induced by dissipation (2023), arXiv:2310.02539 [cond-mat.supr-con].
- [37] S. Banerjee and M. S. Scheurer, Enhanced superconducting diode effect due to coexisting phases, *Phys. Rev. Lett.* **132**, 046003 (2024).
- [38] A. L. Sharpe, E. J. Fox, A. W. Barnard, J. Finney, K. Watanabe, T. Taniguchi, M. A. Kastner, and D. Goldhaber-Gordon, Emergent ferromagnetism near three-quarters filling in twisted bilayer graphene, *Science* **365**, 605 (2019).
- [39] M. Serlin, C. L. Tschirhart, H. Polshyn, Y. Zhang, J. Zhu, K. Watanabe, T. Taniguchi, L. Balents, and A. F. Young, Intrinsic quantized anomalous Hall effect in a moiré heterostructure, *Science* **367**, 900 (2020).
- [40] Y. Su and S.-Z. Lin, Current-induced reversal of anomalous Hall conductance in twisted bilayer graphene, *Phys. Rev. Lett.* **125**, 226401 (2020).
- [41] X. Ying, M. Ye, and L. Balents, Current switching of valley polarization in twisted bilayer graphene, *Phys. Rev. B* **103**, 115436 (2021).
- [42] W.-Y. He, D. Goldhaber-Gordon, and K. T. Law, Giant orbital magnetoelectric effect and current-induced magnetization switching in twisted bilayer graphene, *Nat. Commun.* **11**, 1650 (2020).
- [43] C. Huang, N. Wei, and A. H. MacDonald, Current-driven magnetization reversal in orbital Chern insulators, *Phys. Rev. Lett.* **126**, 056801 (2021).
- [44] U. Zondiner, A. Rozen, D. Rodan-Legrain, Y. Cao, R. Queiroz, T. Taniguchi, K. Watanabe, Y. Oreg, F. von Oppen, A. Stern, E. Berg, P. Jarillo-Herrero, and S. Ilani, Cascade of phase transitions and Dirac revivals in magic-angle graphene, *Nature (London)* **582**, 203 (2020).
- [45] H. Zhou, L. Holleis, Y. Saito, L. Cohen, W. Huynh, C. L. Patterson, F. Yang, T. Taniguchi, K. Watanabe, and A. F. Young, Isospin magnetism and spin-polarized superconductivity in Bernal bilayer graphene, *Science* **375**, 774 (2022).
- [46] H. Zhou, T. Xie, A. Ghazaryan, T. Holder, J. R. Ehrets, E. M. Spanton, T. Taniguchi, K. Watanabe, E. Berg, M. Serbyn, and A. F. Young, Half- and quarter-metals in rhombohedral trilayer graphene, *Nature (London)* **598**, 429 (2021).
- [47] E. C. Stoner and R. Whiddington, Collective electron specific heat and spin paramagnetism in metals, *Proc. R. Soc. Lond. A* **154**, 656 (1936).
- [48] S. Datta, *Electronic Transport in Mesoscopic Systems* (Cambridge University Press, England, 1995).
- [49] J.-X. Hu, Z.-T. Sun, Y.-M. Xie, and K. T. Law, Josephson diode effect induced by valley polarization in twisted bilayer graphene, *Phys. Rev. Lett.* **130**, 266003 (2023).
- [50] N. J. Zhang, J.-X. Lin, D. V. Chichinadze, Y. Wang, K. Watanabe, T. Taniguchi, L. Fu, and J. I. A. Li, Angle-resolved transport non-reciprocity and spontaneous symmetry breaking in twisted trilayer graphene,

- Nat. Mater. **23**, 356 (2024).
- [51] P. Fulde and R. A. Ferrell, Superconductivity in a strong spin-exchange field, *Phys. Rev.* **135**, A550 (1964).
- [52] During applying the current,  $\tilde{\mu}$  should be almost unchanged considering the electron occupation  $n$  is fixed in our case. Therefore, we fix the value of  $\tilde{\mu}$  as the initial modified chemical potential  $\tilde{\mu}^0$  in the calculations. In addition, since the variation of  $h_v$  is also not very large for a small current, we also ignore the influence of  $h_v$  in the parameter  $\alpha_+ - \alpha_-$  when  $h_v$  changes in Eq. (5).
- [53] In all calculated results, we discard both  $I_{c\pm}^1$  as long as one of the  $I_{c\pm}^1$  is smaller than 0.01 which roughly corresponds to 1nA for a narrow bandwidth with  $4t = 10meV$ , considering it is too small to measure in the experiment.
- [54] Y. Cao, J. M. Park, K. Watanabe, T. Taniguchi, and P. Jarillo-Herrero, Pauli-limit violation and re-entrant superconductivity in moiré graphene, *Nature (London)* **595**, 526 (2021).
- [55] E. Lake and T. Senthil, Reentrant superconductivity through a quantum lifshitz transition in twisted trilayer graphene, *Phys. Rev. B* **104**, 174505 (2021).
- [56] D. Xiao, G.-B. Liu, W. Feng, X. Xu, and W. Yao, Coupled spin and valley physics in monolayers of MoS<sub>2</sub> and other Group-VI dichalcogenides, *Phys. Rev. Lett.* **108**, 196802 (2012).
- [57] B. T. Zhou, K. Taguchi, Y. Kawaguchi, Y. Tanaka, and K. T. Law, Spin-orbit coupling induced valley Hall effects in transition-metal dichalcogenides, *Commun. Phys.* **2**, 26 (2019).
- [58] Y. Cao, V. Fatemi, A. Demir, S. Fang, S. L. Tomarken, J. Y. Luo, J. D. Sanchez-Yamagishi, K. Watanabe, T. Taniguchi, E. Kaxiras, R. C. Ashoori, and P. Jarillo-Herrero, Correlated insulator behaviour at half-filling in magic-angle graphene superlattices, *Nature (London)* **556**, 80 (2018).
- [59] Y. Cao, V. Fatemi, S. Fang, K. Watanabe, T. Taniguchi, E. Kaxiras, and P. Jarillo-Herrero, Unconventional superconductivity in magic-angle graphene superlattices, *Nature (London)* **556**, 43 (2018).
- [60] E. Codecido, Q. Wang, R. Koester, S. Che, H. Tian, R. Lv, S. Tran, K. Watanabe, T. Taniguchi, F. Zhang, M. Bockrath, and C. N. Lau, Correlated insulating and superconducting states in twisted bilayer graphene below the magic angle, *Sci. Adv.* **5**, eaaw9770 (2019).
- [61] V. T. Phong, P. A. Pantaleón, T. Cea, and F. Guinea, Band structure and superconductivity in twisted trilayer graphene, *Phys. Rev. B* **104**, L121116 (2021).
- [62] S. Blundell, *Magnetism in Condensed Matter* (Oxford University Press, 2001).
- [63] F. Fiorillo, C. Appino, and M. Pasquale, Chapter 1 - hysteresis in magnetic materials, in *The Science of Hysteresis* (Academic Press, Oxford, 2006) pp. 1–190.
- [64] G. Bertotti, *Hysteresis in Magnetism* (Academic Press, 1998).
- [65] L. Dante, G. Durin, A. Magni, and S. Zapperi, Low-field hysteresis in disordered ferromagnets, *Phys. Rev. B* **65**, 144441 (2002).
- [66] L. Rayleigh, Xxv. notes on electricity and magnetism.—iii. on the behaviour of iron and steel under the operation of feeble magnetic forces, *Philos. Mag.* **23**, 225 (1887).